PHYSICAL REVIEW D **95,** 094014 (2017)

$Z(3)$ metastable states in a Polyakov quark meson model

Ranjita K. Mohapatra* and Hiranmaya Mishra†

Theory Division, Physical Research Laboratory, Navrangpura, Ahmedabad 380009, India

(Received 16 March 2017; published 22 May 2017)

We study the existence of $Z(3)$ metastable states in the presence of the dynamical quarks within the ambit of a Polyakov quark meson (PQM) model. Within the parameters of the model, it is seen that for temperatures T_m greater than the chiral transition temperature T_c, $Z(3)$ metastable states exist ($T_m \sim 310$ MeV at zero chemical potential). At finite chemical potential T_m is larger than the same at vanishing chemical potential. We also observe a shift of ($\sim 5°$) in the phase of the metastable vacua at zero chemical potential. The energy density difference between true and $Z(3)$ metastable vacua is very large in this model. This indicates a strong explicit symmetry-breaking effect due to quarks in the PQM model. We compare this explicit symmetry breaking in the PQM model with small explicit symmetry breaking as a linear term in a Polyakov loop added to the Polyakov loop potential. We also study the possibility of domain growth in a quenched transition to quark gluon plasma in relativistic heavy ion collisions.

DOI: 10.1103/PhysRevD.95.094014

I. INTRODUCTION

The structure of QCD vacuum and its modification under an extreme environment has been a major theoretical and experimental challenge in strong interaction physics. Heavy ion collisions at the Relativistic Heavy Ion Collider (RHIC) and the Large Hadron Collider (LHC) provide an opportunity to investigate modification of the vacuum structure of QCD as related to nonperturbative aspects of QCD. There has been strong evidence that a strongly interacting quark gluon plasma (QGP) is produced in these experiments. With the increase in collision center-of-mass energy from RHIC to LHC, a QGP state at higher temperature $\sim 2T_c$ is expected to be formed at LHC [1]. At such high temperature, it is important to study the nontrivial vacuum structure of QCD arising from $Z(3)$ center symmetry of QCD [2]. In pure $SU(3)$ gauge theory, which can be considered QCD with infinitely heavy quark masses, the confining phase is center symmetric with a vanishing expectation value of the Polyakov loop order parameter. On the other hand, the deconfinement is characterized by a nonvanishing value of the order parameter with three degenerate vacua corresponding to three different phases of $Z(3)$ center symmetry. However, for real QCD with the inclusion of dynamical quarks, $Z(3)$ center symmetry is explicitly broken in the deconfined phase with one true vacuum and two metastable vacua [3–5]. It is generally believed that the explicit symmetry-breaking effect due to quarks is small and a linear term in the Polyakov loop is added to the Polyakov loop potential to take this effect into account [6,7]. For these models, metastable states exist at any temperature greater than T_c. However, some recent lattice QCD results [8] show that these metastable states do not exist in the neighborhood of $T_c(\sim 200$ MeV), but for temperatures $T \geq 750$ MeV. This leads to a strong explicit symmetry breaking rather than small explicit symmetry breaking due to quarks.

It has been studied that these $Z(3)$ domains give a microscopic explanation for the large color opacity (jet quenching) and near perfect fluidity (small value of η/s) of QGP [9,10]. Hence, it is important to study these domains in the nonperturbative regime of QCD in which the system exists in a strongly interacting QGP phase just after the collision of two heavy nuclei in relativistic heavy ion collisions. Due to the explicit symmetry effect of quarks, there are huge oscillations in the Polyakov loop order parameter field which give rise to large fluctuations in the flow anisotropies in the quenched transition to QGP [11]. The importance of $Z(3)$ walls has also been discussed as nontrivial scattering of quarks from $Z(3)$ walls. Its consequences for cosmology as well as for heavy ion collision have been explored [12–15], including the possibility of CP-violating scattering of quarks from $Z(3)$ walls leading to interesting observational implications [16].

These $Z(3)$ metastable states have been studied at high temperatures in the presence of dynamical quarks [3,5]. It has been shown that the contribution of massless quarks to the one-loop effective potential leads to metastable states and the free energy density difference between true and metastable vacua is given by $\frac{2}{3}\pi^2 T^4 \frac{N_f}{N^3}(N^2-2)$, with N_f and N being the number of light flavors and number of colors, respectively. Since the calculation of the effective potential here is perturbative, it is only valid at temperatures much larger than Λ_{QCD}. We do not expect it to be valid near T_c. However, a detailed description of such metastable states near T_c is difficult both because of the nonperturbative nature of QCD and the incompleteness of the theory of thermodynamics of the nonequilibrium systems.

*ranjita.iop@gmail.com
†hm@prl.res.in

Therefore, in the present work, we examine these metastable states near T_c using the Polyakov quark meson (PQM) model [17]. This model is based on the two important aspects of the QCD phase transition, chiral transition and confinement-deconfinement phase transition. The Polyakov loop potential represents the SU(3) pure gauge theory part which respects $Z(3)$ center symmetry. The linear sigma model is included to represent the chiral symmetry of QCD. The quarks are minimally coupled to a spatially constant temporal background gauge field A_0. The model thus cleverly uses the chiral as well as confining properties of QCD. Since the constituent quark masses are much larger than the mass of pions, the meson dynamics dominate at low temperatures, reproducing the results of chiral perturbation theory. Since this model describes an interaction potential among quarks, mesons, and the Polyakov loop, this is a very suitable model to study the metastable states near T_c.

It has been shown that the sign of finite temperature correction to the effective potential depends on the sign of the real part of the Polyakov loop [5]. In general, it gives a negative contribution to the energy density of the vacuum when the real part of the Polyakov loop is positive (making it a global minimum for $\theta = 0$). However, it gives a positive contribution to the effective potential (making it metastable) when the real part of the Polyakov loop is negative. This is also the case for the PQM model. The Polyakov loop potential respects $Z(3)$ symmetry and there are three degenerate vacua at any temperature greater than the critical temperature. However, when the interaction term between the Polyakov loop and quarks is included as given in PQM model, the $\theta = 0$ vacuum becomes true vacuum due to the addition of a negative energy density, since the real part of the Polyakov loop is positive. The other two $Z(3)$ vacua become metastable due to the addition of a positive energy density, since the real part of the Polyakov loop is negative. Since the interaction part between the Polyakov loop and quarks in the PQM model also has chemical potential dependence, we study these metastable states, along with their temperature and chemical potential dependence, in great detail in this model. In this paper, we also have shown that, of different forms of the Polyakov loop potentials those with a large barrier between different $Z(3)$ vacuums sustain the $Z(3)$ metastability structure when the interaction term between quarks and the Polyakov loop is added.

It is important and relevant to study nonequilibrium effects since there are metastable states in the system. In classical nonequilibrium thermodynamics, metastable states play a crucial role in explaining various phenomena like supercooling and supersaturation. In analogy, one might expect interesting phenomenology of topological supercooling of QGP in heavy ion collisions. This has been already studied as a numerical simulation in Ref. [11], where the phase transition from the confined to deconfined phase is modeled by a quench to a very high temperature within the Polyakov loop potential. The evolution of $Z(3)$ domains has been studied for different cases like those with small or large explicit symmetry-breaking effects by putting a small or large term as the coefficient of the linear term in the Polyakov loop potential [11]. In the present investigation, we discuss domain growth for the Polyakov loop and the quark condensate order parameter in a quench scenario. The nonequilibrium effects have been studied using Langevin equations within different effective models of QCD like the PQM model [18], as well as the Nambu–Jona-Lasinio (NJL) model [19].

The paper is organized in the following manner. In Sec. II, we discuss the essential aspects of the PQM model. Here, we discuss the two different parametrizations used in the literature for the Polyakov loop potential in SU(3) pure gauge theory. Section III describes the metastable states at higher temperature and chemical potential. It is shown that the parametrization for the pure gauge part, which has a larger barrier between different vacua, leads to the existence of metastable states when quarks are coupled to it. We show that there is a large symmetry-breaking effect due to quarks, which leads to the existence of metastable states at higher temperature and a large shift ($\sim 5°$) in the phase of metastable vacua. We compare the explicit symmetry breaking of the PQM model with small explicit symmetry breaking as a linear term in the Polyakov loop added to the Polyakov loop potential. Section IV discusses the numerical techniques for the simulation to describe the phase transition via quench and the results of the simulation. Finally, in Sec. V, we summarize the results of the present investigation and give a possible outlook.

II. THE POLYAKOV-QUARK-MESON MODEL

A. The Polyakov loop potential

The thermal expectation value of the Polyakov loop represents the order parameter for the confinement-deconfinement phase transition. The Polyakov loop operator is a Wilson loop in the temporal direction

$$\mathcal{P} = P \exp\left(i \int_0^\beta dx_0 A_0(x_0)\right), \tag{1}$$

where $A_0(x_0)$ is the temporal component of the gauge field A_μ, P denotes path ordering in the Euclidean time τ, and $\beta = 1/T$, with T being the temperature. Within the Polyakov gauge, the temporal component of the gauge field is time independent, so that $\mathcal{P} = \exp(i\beta A_0)$. Further, one can rotate the gauge field in the Cartan subalgebra $A_0^c = A_0^3\lambda_3 + A_0^8\lambda_8$. The normalized Polyakov loop variable Φ and its charge conjugate $\bar{\Phi}$ are defined as the color trace of the Polyakov loop operator defined in Eq. (1):

$$\Phi = \frac{1}{N_c}\mathrm{tr}\mathcal{P}, \qquad \bar{\Phi} = \frac{1}{N_c}\mathrm{tr}\mathcal{P}^\dagger. \tag{2}$$

Here the trace is taken in the fundamental representation. Φ and $\bar{\Phi}$ are complex scalar fields and their mean values are related to the free energy of infinitely heavy, static quarks or antiquarks. The order parameter Φ vanishes in the confined phase since an infinite amount of free energy is required to put a static quark in that phase. However, the order parameter is finite in the deconfined phase related to the finite free energy of static quarks.

Under $Z(\mathrm{N})$ center symmetry of SU(N) gauge symmetry, the Polyakov loop order parameter transforms as

$$\Phi \to z\Phi, \qquad z \in Z(N) \tag{3}$$

In pure SU(3) gauge theory which is the limit of QCD with infinitely heavy quarks, the confining phase is center symmetric so that $\langle\Phi\rangle = 0$, whereas deconfinement is characterized by a nonvanishing value of the Polyakov loop expectation value, since center symmetry is broken spontaneously. In the physical world, with finite quark masses, this symmetry is explicitly broken.

For SU(3) pure gauge theory, the effective potential of the Polyakov loop has been proposed with the parameters fitted to reproduce lattice results for pressure and energy density. Let us note here that the explicit form of the Polyakov loop is not known directly from first principle calculations. The approach has been to choose a functional form that reproduces crucial features of pure gauge theory and adjust the parameters of the function so as to reproduce the thermodynamical observables of lattice simulations. Here, we will discuss two kinds of parametrization used in the literature as discussed below. The parameter set 1 is taken from Ref. [6] and the parameter set 2 is taken from Refs. [17,20]. Both the potentials with the parameters given below represent a first-order phase transition at the critical temperature $\mathrm{T}_0 = 270$ MeV. For the parameter set 1, the effective Polyakov potential is given by

$$\frac{\mathcal{U}(\Phi,\bar{\Phi})}{\mathrm{T}^4} = \left(-\frac{b_2}{4}(|\Phi|^2+|\bar{\Phi}|^2) - \frac{b_3}{6}(\Phi^3+\bar{\Phi}^3) + \frac{1}{16}(|\Phi|^2+|\bar{\Phi}|^2)^2\right) * b_4. \tag{4}$$

The moduli of Φ and $\bar{\Phi}$ are the same for pure gauge theory. By writing $\Phi = |\Phi|e^{i\theta}$, one can see that the b_3 term in Eq. (4) gives the $\cos 3\theta$ term leading to $Z(3)$ degenerate vacua for a nonvanishing value for $|\Phi|$ i.e. for temperatures greater than the critical temperature T_0. The coefficients b_3 and b_4 have been taken as $b_3 = 2.0$ and $b_4 = 0.6016$. The temperature-dependent coefficient b_2 is

$$b_2(\mathrm{T}) = (1 - 1.11 * \mathrm{T}_0/\mathrm{T})(1 + 0.265 * \mathrm{T}_0/\mathrm{T})^2 \times (1 + 0.3 * \mathrm{T}_0/\mathrm{T})^3 - 0.487. \tag{5}$$

With the coefficients chosen as above, the expectation value of the order parameter approaches $x = b_3/2 + \frac{1}{2}\sqrt{b_3^2 + 4b_2(\mathrm{T}=\infty)}$ for temperature $\mathrm{T} \to \infty$. We use the normalization such that the expectation value of the order parameter Φ goes to unity for temperature $\mathrm{T} \to \infty$. Hence the fields and the coefficients in the above potential are rescaled as $\Phi \to \Phi/x$, $b_2(\mathrm{T}) \to b_2(\mathrm{T})/x^2$, $b_3 \to b_3/x$, and $b_4 \to b_4 x^4$ to get the proper normalization of Φ.

For the parameter set 2, the effective Polyakov potential is

$$\frac{\mathcal{U}(\Phi,\bar{\Phi})}{\mathrm{T}^4} = -\frac{b_2}{4}(|\Phi|^2+|\bar{\Phi}|^2) - \frac{b_3}{6}(\Phi^3+\bar{\Phi}^3) + \frac{b_4}{16}(|\Phi|^2+|\bar{\Phi}|^2)^2. \tag{6}$$

Here, the temperature-independent coefficients $b_3 = 0.75$, $b_4 = 7.5$ and temperature-dependent coefficient b_2 is given by

$$b_2(\mathrm{T}) = a_0 + a_1\left(\frac{\mathrm{T}_0}{\mathrm{T}}\right) + a_2\left(\frac{\mathrm{T}_0}{\mathrm{T}}\right)^2 + a_3\left(\frac{\mathrm{T}_0}{\mathrm{T}}\right)^3 \tag{7}$$

where $a_0 = 6.75$, $a_1 = -1.95$, $a_2 = 2.625$, and $a_3 = -7.44$.

The difference between these two parametrizations is that the barrier between $Z(3)$ vacua for parameter set 1 is very large compared to that of parameter set 2 at any temperature greater than T_0. Figure 1 shows the barrier between different $Z(3)$ vacua at a temperature $\mathrm{T} = 400$ MeV at the corresponding vacuum expectation value of the Polyakov potential. Here the parameters are such that the vacuum expectation values of the Polyakov potential at $\mathrm{T} = 400$ MeV for parameter set 1 and set 2 are 0.92 and 0.81, respectively. The energy density is almost equal for different $Z(3)$ vacua for both cases.

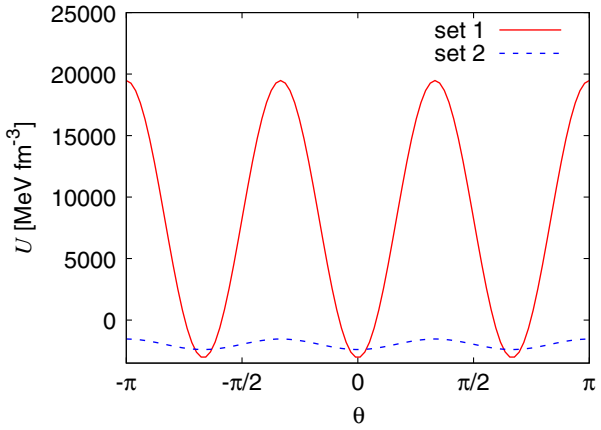

FIG. 1. The $Z(3)$ structure of the vacuum in the plot of the Polyakov potential for both parameter sets as a function of θ at a temperature 400 MeV.

In the deconfined phase, due to the breaking of $Z(3)$ symmetry, one gets domain walls or interfaces that interpolate between different $Z(3)$ vacua. We can also see that the $Z(3)$ interface profile will be different for the Polyakov loop potential described by set 1 and set 2. The $Z(3)$ interface arises as one goes from one $Z(3)$ vacuum to another $Z(3)$ vacuum. These interfaces have been well studied in SU(3) lattice pure gauge theory [21]. The interface solution for the Polyakov loop potential as a time-independent solution is given in [12]. Here, we also use the same energy minimization technique as in [12] to get the interface profile. To determine the interface profile one needs to consider the profile of the Polyakov loop in one dimension (say along z). We fix the values of Φ at the two boundaries of the one-dimensional lattice as the values of the Polyakov loop corresponding to two distinct minima [two $Z(3)$ degenerate minima] of the Polyakov potential. Field configuration is then fluctuated at each lattice point, while fixing the boundary points, and energy is minimized. The configuration with the lowest value of energy is accepted (when the energy almost settles down to a definite value) as the correct profile of the interface. We refer to [12] for the details of the energy minimization technique. For the Polyakov loop potential with parameter set 1, the minimum energy configuration is such that the Polyakov order parameter goes very close to $\Phi = 0$, since there is a huge barrier between different $Z(3)$ vacua. This is also seen in lattice gauge theory [21]. However, for the potential with parameter set 2, the barrier between different $Z(3)$ vacua is even smaller than the central bump near $\Phi = 0$. So for the potential set 2, the minimum energy configuration going from one vacuum to another vacuum never goes close to $\Phi = 0$; rather it goes through a path where the modulus of Φ remains almost constant and θ is continuously changing. The profile of the interface in the complex plane of the Polyakov loop order parameter at a temperature of 500 MeV ($\sim 2T_0$) for both parameter sets is shown in Fig. 2.

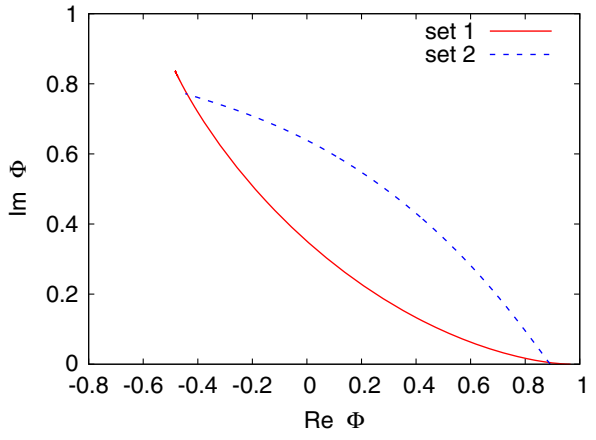

FIG. 2. The path of the Polyakov order parameter Φ in the complex plane when crossing the $Z(3)$ interface at a temperature of 500 MeV. This path corresponds to a minimum energy configuration as one goes from one vacuum to another $Z(3)$ vacuum.

There is another possible parametrization used in the literature for the Polyakov loop potential called logarithmic parametrization, given by [22]

$$\frac{\mathcal{U}_{\log}(\Phi,\bar{\Phi})}{\mathrm{T}^4} = -\frac{1}{2}A(\mathrm{T})\bar{\Phi}\Phi + B(\mathrm{T})\ln[1 - 6(\bar{\Phi}\Phi) + 4(\Phi^3 + (\bar{\Phi})^3) - 3(\bar{\Phi}\Phi)^2]. \tag{8}$$

Here, the temperature-dependent coefficients are given by

$$A(\mathrm{T}) = a_0 + a_1\left(\frac{\mathrm{T}_0}{\mathrm{T}}\right) + a_2\left(\frac{\mathrm{T}_0}{\mathrm{T}}\right)^2 \tag{9}$$

and

$$B(\mathrm{T}) = b_3\left(\frac{\mathrm{T}_0}{\mathrm{T}}\right)^3. \tag{10}$$

The different parameters here are $a_0 = 3.51$, $a_1 = -2.47$, $a_2 = 15.2$, and $b_3 = -1.75$.

In this parametrization, the barrier between different $Z(3)$ vacua is not well defined at a temperature greater than T_0 as the argument of the logarithm in Eq. (8) can become negative. Further, the $Z(3)$ structure of the vacuum at the vacuum expectation value as a function of θ is not well defined for this logarithmic potential. Since we are interested in the details of the $Z(3)$ parametrization structure, we do not consider this parametrization here.

In general, the Polyakov loop potential with parameter set 2 is more commonly used in the context of the PQM model because one is interested in the study of thermodynamic equilibrium properties of the system along the true vacuum [17,18,23]. On the other hand, since we are interested in $Z(3)$ metastability and the evolution of $Z(3)$ domains with dynamical quarks, we use the Polyakov loop potential with parameter set 1 throughout this paper. We will also see later in the paper that including the quark contribution to the Polyakov loop potential washes away $Z(3)$ metastability structure for parameter set 2. This is primarily because the barrier between different $Z(3)$ vacua is very small for the parameter set 2. Since the barrier between different $Z(3)$ vacua is very large for parameter set 1, the quark effect does not wash away the $Z(3)$ metastability structure.

B. Quark-meson coupling to Polyakov loop

Chiral symmetry of QCD is an important symmetry to understand low-energy hadronic properties [24]. There are different phenomenological models like the NJL and quark-meson (QM) model that are based on this chiral symmetry of QCD. By combining the Polyakov loop model with the QM model, both the confining and chiral properties of QCD are included.

The Lagrangian of the linear QM model for $N_f = 2$ light quarks $q = (u, d)$ and $N = 3$ color degrees of freedom coupled minimally to a spatially constant temporal background gauge field is given by

$$\mathcal{L} = \bar{q}[(i\gamma^\mu\partial_\mu - ig_s\gamma^0 A_0) - g(\sigma + i\gamma_5\vec{\tau}\vec{\pi})]q + \frac{1}{2}(\partial_\mu\sigma)^2 + \frac{1}{2}(\partial_\mu\vec{\pi})^2 - U(\sigma,\vec{\pi}) - \mathcal{U}(\Phi,\bar{\Phi}) \quad (11)$$

where the linear sigma model potential reads

$$U(\sigma,\vec{\pi}) = \frac{\lambda}{4}(\sigma^2 + \vec{\pi}^2 - v^2)^2 - c\sigma. \quad (12)$$

The parameters in Eq. (12) are chosen such that chiral symmetry is spontaneously broken in vacuum, where $\langle\sigma\rangle = f_\pi = 93$ MeV, and here f_π is the pion decay constant. Since pions are pseudoscalar in character, the expectation values vanish $\langle\vec{\pi}\rangle = 0$. The explicit symmetry-breaking term is $c \sim 1.77 \times 10^6$ MeV^3 which produces a pion mass of 138 MeV. The quartic coupling λ is given by sigma mass m_σ by the relation $\lambda = (m_\sigma^2 - m_\pi^2)/2f_\pi^2$. In the present calculations, we take $m_\sigma = 600$ MeV, leading to $\lambda \simeq 20$. The parameter v^2 is found by minimizing the potential in the radial direction $v^2 = \sigma^2 - c/(\lambda\sigma)$. Finally, the Yukawa coupling constant $g = 3.2$, which is fixed to produce a constituent quark mass of 300 MeV in the vacuum $m_q = gf_\pi$.

The partition function $\mathcal{Z}$ is written as a path integral over quarks, antiquarks, mesons, and the temporal component of the gauge field. We shall adopt here a mean field approximation of replacing the meson and the Polyakov loop fields by their vacuum expectation values. This amounts to neglecting both the quantum and thermal fluctuations of all the fields other than the quark and antiquark fields. Integrating over the quark degrees of freedom, one can get the thermodynamic potential. The effective thermodynamic potential is determined as the logarithm of the partition function,

$$V_{\text{eff}} = -\frac{\mathrm{T}}{\mathrm{V}}\ln\mathcal{Z} = \mathcal{U}(\Phi,\bar{\Phi}) + U(\sigma) + \Omega_{\bar{q}q}(\Phi,\bar{\Phi},\sigma), \quad (13)$$

where

$$\Omega_{\bar{q}q} = -2N_f\mathrm{T}\int\frac{d^3p}{(2\pi)^3}\ln\left[1 + 3(\Phi + \bar{\Phi}e^{-(E_p-\mu)/\mathrm{T}})e^{-(E_p-\mu)/\mathrm{T}} + e^{-3(E_p-\mu)/\mathrm{T}}\right] + \ln\left[1 + 3(\bar{\Phi} + \Phi e^{-(E_p+\mu)/\mathrm{T}})e^{-(E_p+\mu)/\mathrm{T}} + e^{-3(E_p+\mu)/\mathrm{T}}\right]. \quad (14)$$

In the above, E_p is the quark or antiquark quasiparticle energy given by $E_p = \sqrt{|\vec{p}|^2 + m_q^2}$ with the constituent quark mass $m_q = g\sigma$. Clearly in Eq. (14) above we have written $\sigma = \langle\sigma\rangle$, $\Phi = \langle\Phi\rangle$, $\bar{\Phi} = \langle\Phi\rangle$ and have taken the pion field as having a vanishing vacuum expectation value. Further, in Eq. (14), we have omitted a zero temperature and density contribution in $\Omega_{\bar{q}q}$ that can be absorbed partly into parameter λ and a logarithmic term depending upon the renormalization scale and effective quark mass. However, the qualitative features of the phase diagram remain unchanged as long as the mass of the sigma meson is not too high [23,25]. We therefore proceed with our analysis without the vacuum fluctuation terms for the fermions in $\Omega_{\bar{q}q}$.

III. $Z(3)$ METASTABILITY IN PQM MODEL

In pure SU(3) gauge theory, the deconfined phase exists in three degenerate states and these three states are related to each other via $Z(3)$ rotation. However, inclusion of dynamical quarks breaks this $Z(3)$ symmetry due to antiperiodic boundary conditions on fermions. Thus, the $Z(3)$ symmetry is explicitly broken giving rise to one true vacuum along $\theta = 0$ and two metastable vacua along $\theta = 2\pi/3$ and $4\pi/3$. In this section, we will discuss these $Z(3)$ metastable states in the context of the PQM model where the effect of quarks is included in terms of the QM model.

To study the dynamics of phase transition within PQM model, it is convenient to write down the effective thermodynamic potential Eq. (13) in terms of the real and imaginary parts of the Polyakov order parameter as in Ref. [23]. Defining $\alpha = (\Phi + \bar{\Phi})/2 = |\Phi|\cos\theta$ and $\beta = (\Phi - \bar{\Phi})/(2i) = |\Phi|\sin\theta$, the Polyakov potential for parameter set 1, i.e., Eq. (4), and set 2, i.e., Eq. (6), can be rewritten as functions of real variables α and β, respectively, as

$$\frac{\mathcal{U}(\alpha,\beta)}{\mathrm{T}^4} = \left(-\frac{b_2}{2}(\alpha^2+\beta^2) - \frac{b_3}{3}(\alpha^3 - 3\alpha\beta^2) + \frac{1}{4}(\alpha^2+\beta^2)^2\right)b_4 \quad (15a)$$

$$\frac{\mathcal{U}(\alpha,\beta)}{\mathrm{T}^4} = \left(-\frac{b_2}{2}(\alpha^2+\beta^2) - \frac{b_3}{3}(\alpha^3 - 3\alpha\beta^2) + \frac{b_4}{16}(\alpha^2+\beta^2)^2\right). \quad (15b)$$

Similarly, defining

$$x_+ \equiv 1 + 3(\Phi + \bar{\Phi}e^{-(E-\mu)/\mathrm{T}})e^{-(E-\mu)/\mathrm{T}} + e^{-3(E-\mu)/\mathrm{T}} \quad (16)$$

and

$$x_- \equiv 1 + 3(\bar{\Phi} + \Phi e^{-(E+\mu)/\mathrm{T}})e^{-(E+\mu)/\mathrm{T}} + e^{-3(E+\mu)/\mathrm{T}}, \quad (17)$$

$$x_+ x_- = R + iI, \quad (18)$$

the contribution $\Omega_{q\bar{q}}$ from the quarks at finite temperature and chemical potential can be written as

$$\Omega_{q\bar{q}} = -2\mathrm{N}_f \mathrm{T} \int \frac{d^3p}{(2\pi)^3} \log[x_+ x_-]. \quad (19)$$

It can be seen that the argument of the logarithm is complex and $x_+ x_- = R + iI$, where

$$\begin{aligned} R \equiv\ & 1 + e^{-3(E-\mu)/\mathrm{T}} + e^{-3(E+\mu)/\mathrm{T}} + e^{-6E/\mathrm{T}} \\ & + 6\alpha e^{-E/\mathrm{T}}\left[\cosh\left(\frac{\mu}{\mathrm{T}}\right) + e^{-E/\mathrm{T}}\cosh\left(\frac{2\mu}{\mathrm{T}}\right)\right] \\ & + 6\alpha e^{-4E/\mathrm{T}}\left[\cosh\left(\frac{2\mu}{\mathrm{T}}\right) + e^{-E/\mathrm{T}}\cosh\left(\frac{\mu}{\mathrm{T}}\right)\right] \\ & + 9(\alpha^2 + \beta^2)(1 + e^{-2E/\mathrm{T}})e^{-2E/\mathrm{T}} \\ & + 18(\alpha^2 - \beta^2)e^{-3E/\mathrm{T}}\cosh\left(\frac{\mu}{\mathrm{T}}\right) \end{aligned} \quad (20)$$

and

$$\begin{aligned} I \equiv\ & 6\beta e^{-E/\mathrm{T}}\left[\sinh\left(\frac{\mu}{\mathrm{T}}\right) - e^{-E/\mathrm{T}}\sinh\left(\frac{2\mu}{\mathrm{T}}\right)\right] \\ & + 6\beta e^{-4E/\mathrm{T}}\left[e^{-E/\mathrm{T}}\sinh\left(\frac{\mu}{\mathrm{T}}\right) - \sinh\left(\frac{2\mu}{\mathrm{T}}\right)\right] \\ & - 36\alpha\beta\sinh\left(\frac{\mu}{\mathrm{T}}\right)e^{-3E/\mathrm{T}}. \end{aligned} \quad (21)$$

In principle, one can write $R + iI = \rho e^{i\delta}$, where

$$\rho \equiv \sqrt{R^2 + I^2} \quad \text{and} \quad \delta \equiv \arctan\left(\frac{I}{R}\right). \quad (22)$$

Thus the potential has an imaginary part and this is the manifestation of the fermion sign problem in the context of the PQM model [23,26]:

$$\Omega_{q\bar{q}} = \Omega^R_{q\bar{q}} + i\Omega^I_{q\bar{q}}, \quad (23)$$

with

$$\Omega^R_{q\bar{q}} \equiv -2\mathrm{N}_f \mathrm{T} \int \frac{d^3p}{(2\pi)^3} \ln[\rho] \quad (24)$$

and

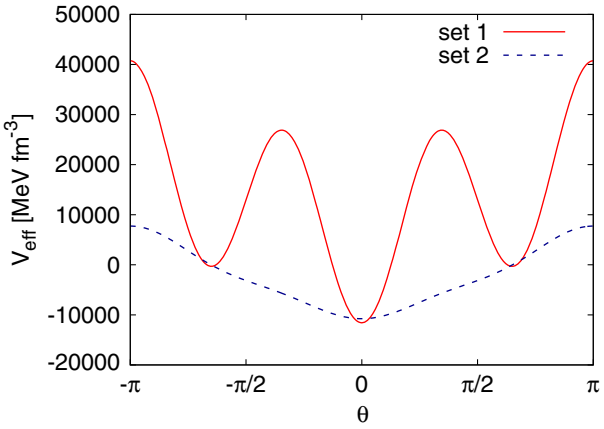

FIG. 3. Effective potential as a function of the phase of the Polyakov loop for T = 400 MeV and $\mu = 0$. Set 1 corresponds to the Polyakov potential of Ref. [6], while set 2 corresponds to Ref. [17].

$$\Omega^I_{q\bar{q}} \equiv -2\mathrm{N}_f \mathrm{T} \int \frac{d^3p}{(2\pi)^3} \delta. \quad (25)$$

A. $Z(3)$ metastable states at zero chemical potential

The imaginary part of the potential, i.e., Eq. (25), vanishes at $\mu = 0$ and the effective potential becomes real. There is no fermion sign problem at zero chemical potential. We will first consider the case with $\mu = 0$. For two flavors, we take the value of T_0 as 210 MeV [17]. When the real part of the Polyakov loop α is positive, $\beta = 0$ (i.e., along $\theta = 0$) and the appropriate σ value corresponding to the temperature $\Omega^R_{q\bar{q}}$ in Eq. (24) becomes negative. So, the total effective potential V_{eff} along $\theta = 0$ is a global minimum and it becomes the true vacuum. However, along the other two $Z(3)$ vacua, when α is negative, $\Omega^R_{q\bar{q}}$ in Eq. (24) is positive. Hence the total effective potential V_{eff} can have metastable vacua along these directions. For the two different Polyakov loop potential sets 1 and 2, the effective potential at the vacuum expectation value of the Polyakov loop potential as a function of θ at temperature 400 MeV is shown in Fig. 3.

From Fig. 3, it is clear that there are no metastable vacua for Polyakov loop potential set 2 since the barrier between different $Z(3)$ vacua is very small for SU(3) pure gauge theory as shown in Fig. 1 and the strong explicit symmetry-breaking effect due to quarks completely washes away the metastable structure. For parameter set 2, the potential is tilted all the way to a $\theta = 0$ vacuum at all temperatures greater than critical temperature. But, this is not the case for the parameter set 1. One can clearly see the metastable and true vacua in the PQM model for the Polyakov loop potential corresponding to set 1. Since we are interested in the $Z(3)$ vacuum structure, we consider the Polyakov loop potential set 1 throughout the paper.

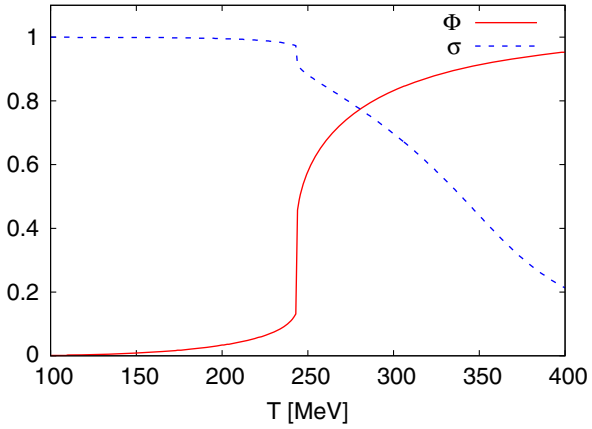

FIG. 4. The normalized chiral condensate σ and the Polyakov loop Φ as a function of temperature.

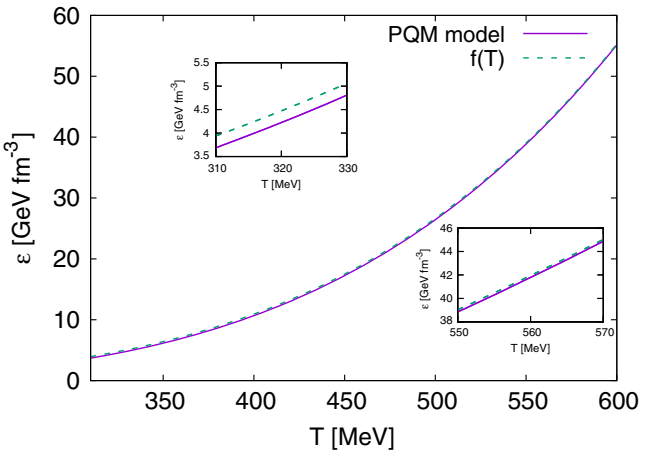

FIG. 5. Free energy density difference between true and metastable vacua as a function of temperature.

By minimizing the effective thermodynamic potential $V_{\rm eff}$ with respect to α, β, and σ,

$$\frac{\partial V_{\rm eff}}{\partial \alpha} = \frac{\partial V_{\rm eff}}{\partial \beta} = \frac{\partial V_{\rm eff}}{\partial \sigma} = 0, \tag{26}$$

we get the global minimum at finite values of α and σ and $\beta = 0$ (along the $\theta = 0$ direction). A comment regarding the above may be relevant. The condition of Eq. (26) is a necessary condition for a minimum and not a sufficient condition. We have verified that the solution is indeed a minimum and does not correspond to a maximum or a saddle point. The variation of the modulus of the Polyakov loop order parameter $|\Phi| = \sqrt{(\alpha^2 + \beta^2)}$ and σ with respect to temperature is shown in Fig. 4. Here, we can see a chiral crossover is found at a temperature $\mathrm{T} = 180$ MeV as also seen in [17]. We also find that Φ reaches a higher value 1.11 as temperature increases [17].

Now using the same σ value at a given temperature that minimizes the effective potential $V_{\rm eff}$, we scan all values of (α, β) corresponding to the second and the third quadrant of the Polyakov loop order parameter to find local minima corresponding to $Z(3)$ metastable vacua. We ascribe the state as metastable when the corresponding pressure is positive and is lower than the pressure at $\theta = 0$. We would like to note here that this procedure is only an approximate method to get a local minimum. In principle, there could be a different pair of (σ, Φ) which can still be metastable with a value of σ other than the value of σ at the minimum with $\theta = 0$. We do not see any $Z(3)$ metastable vacua up to a temperature of 310 MeV; i.e., the free energy density is still higher than the free energy density in the confined phase. At a temperature of 310 MeV and beyond, $Z(3)$ metastable vacua start appearing. However, there is a large difference of free energy density ($\epsilon \sim 4.0$ GeV fm^{-3}) between true and $Z(3)$ metastable vacua at this temperature. This energy difference between metastable and true vacua increases as temperature increases as shown in Fig. 5. It has been already shown that the free energy density difference between true and metastable vacua varies as $\frac{2}{3}\pi^2 \mathrm{T}^4 \frac{\mathrm{N}_l}{\mathrm{N}^3}(\mathrm{N}^2 - 2)$ using the perturbative calculation [3]. Here, $\mathrm{N}_l = 2$ is the number of massless fermions and $\mathrm{N} = 3$ is the number of colors. In Fig. 5, we have fitted the plot by using the same function $f(\mathrm{T}) = \frac{2}{3}\pi^2 \mathrm{T}^4 \frac{\mathrm{N}_l}{\mathrm{N}^3}(\mathrm{N}^2 - 2)$. This function fits with the PQM model extraordinarily well beyond temperature 550 MeV (as shown in the inset). However, near temperature ~310 MeV when $Z(3)$ metastable vacua start appearing, this function does not fit well with data. The difference in the free energy density is ~0.3 GeV fm^{-3} near temperature 310 MeV. This is mainly because the functional dependence given above comes from perturbative calculations, which is valid at higher temperatures.

Further, there is a shift in the phase of the Polyakov loop for the metastable vacua of the order of 5° (metastable vacua appear at angles 115° and 245°). The magnitude of Φ along the metastable vacua is also smaller than the magnitude along the true vacuum. We show contour plots of the effective potential $V_{\rm eff}$ as a function of real and imaginary parts of the Polyakov loop at different temperatures in Fig. 6. Here the value of σ is taken as the value which minimizes the effective potential $V_{\rm eff}$ at the corresponding temperature. The maximum value of $V_{\rm eff}$ is set as 6.3 GeV fm^{-3} in all figures to show the true, metastable vacua and the barrier between them distinctively. Figure 6(a) shows the contour plot of the effective potential at temperature 300 MeV and we can clearly see that there are no $Z(3)$ metastable vacua at this temperature since the energy density of metastable vacuum is still positive (i.e., larger than the energy density in the confined phase). Figure 6(b) represents the effective potential at temperature 400 MeV, and $Z(3)$ metastable vacua and true vacuum are clearly seen at this temperature.

Next, we examine another case where the explicit symmetry-breaking effect due to quarks is included as a

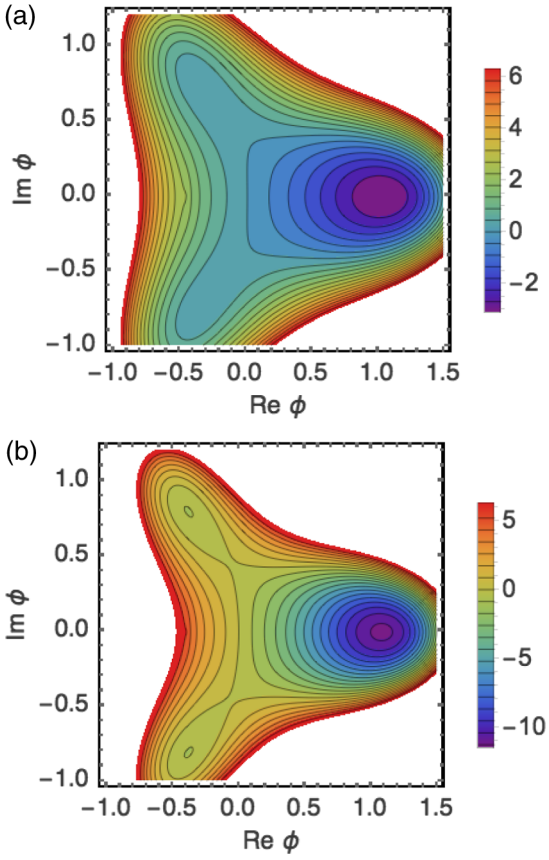

FIG. 6. Contour plot of effective potential at temperatures (a) 300 MeV and (b) 400 MeV. The legend bar represents energy density in GeV fm^{-3}.

linear term in the Polyakov loop in the Polyakov potential given in Eq. (4) [6]. We will compare here the explicit symmetry-breaking effects for this case with the PQM model. The Polyakov loop potential with an explicit symmetry-breaking term is given by [6]

$$\frac{\mathcal{U}_e(\Phi,\bar{\Phi})}{T^4} = \left(-b_1(|\Phi|)\cos\theta - \frac{b_2}{4}(|\Phi|^2+|\bar{\Phi}|^2) - \frac{b_3}{6}(\Phi^3+\bar{\Phi}^3) + \frac{1}{16}(|\Phi|^2+|\bar{\Phi}|^2)^2\right) * b_4. \tag{27}$$

Here, b_1 is the explicit symmetry-breaking term that takes values in the range from 0 to 0.12, as shown in Ref. [6]. While for small b_1 ($b_1 < 0.026$), the weakly first-order transition of pure gauge theory persists, the same becomes a crossover for larger values of b_1. For comparison with the PQM model where the transition is a crossover, we have taken a value $b_1 = 0.1$. Further, to take into account the flavor effect, the parameter b_4 is multiplied by a factor $37/16$ to its pure gauge value. In Ref. [6], it was shown that this explicit symmetry-breaking linear term is sufficient to describe the dependence of the chiral

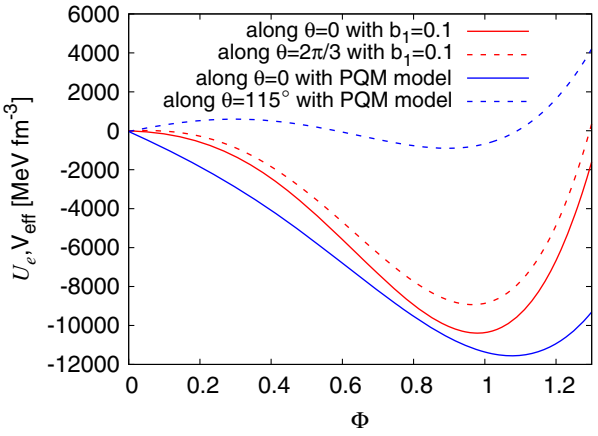

FIG. 7. The Polyakov loop potential with explicit symmetry-breaking term $\mathcal{U}_e$ [Eq. (27)] and the effective potential V_{eff} of the PQM model [Eq. (13)] as a function of Φ along true and metastable vacua at T = 400 MeV.

symmetry restoration temperature on pion mass. For this potential given in Eq. (27), $Z(3)$ metastable vacua are there at all temperatures greater than the critical temperature and the phase shift of the metastable vacuum is negligible.

In Fig. 7 we have plotted the explicit symmetry-breaking potential $\mathcal{U}_e$ of Eq. (27) for $\theta = 0$ corresponding to the stable vacuum and for $\theta = 2\pi/3$ corresponding to metastable vacuum at a temperature 400 MeV as a function of the order parameter $|\Phi|$. These are shown by the red lines. In the same figure we have also plotted the V_{eff} of Eq. (13), along with the corresponding curves for the stable ($\theta = 0$) and metastable ($\theta = 115°$) vacuum. This is because, as mentioned earlier, the metastable vacuum for the PQM case occurs with a shift of 5°.

It is clear from the figure that the free energy density difference between true and $Z(3)$ metastable vacuum is very small in the case of the small explicit symmetry-breaking term used in [6], as compared to the PQM model. Thus, the PQM model shows strong explicit breaking effects due to quarks. Further, the energy density difference along metastable and true vacuum near $\Phi = 0$ is large in the PQM model compared to the potential in Eq. (27). This will have important consequences for the phase transition kinetics for these two cases as we shall see in the next section. We will see later in the simulation that when the explicit symmetry breaking is small [6] with $b_1 = 0.1$, $Z(3)$ domains are formed during the initial time of evolution after quenching the system to a higher temperature of 400 MeV. Subsequently the metastable domains collapse and true vacuum domains expand due to the difference in free energy between them. On the other hand, for the PQM model, after the quench the whole system evolves into true vacuum rapidly. For the large explicit symmetry breaking in the PQM model, we do not get any metastable domains in the simulation. However, this is not the case with the small explicit symmetry-breaking effect used in [6]. This will be discussed later in detail in the next section.

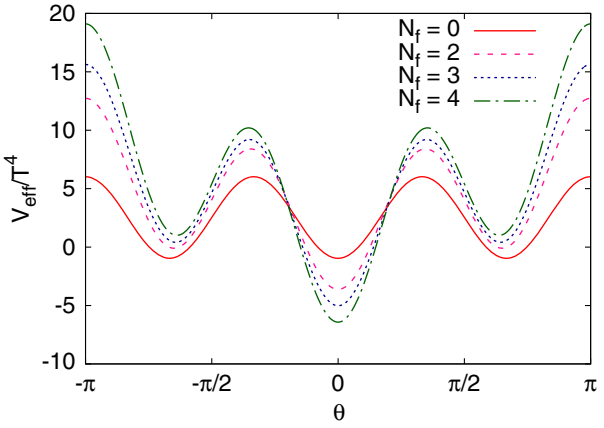

FIG. 8. V_{eff} as a function of θ for different numbers of flavors at $T = 400$ MeV.

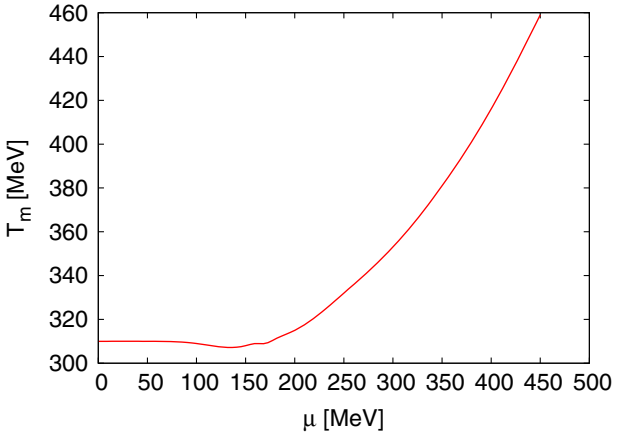

FIG. 9. The temperature T_m beyond which $Z(3)$ metastable vacuum occurs as a function of chemical potential.

Here we would like to explore another interesting possibility of the dependence of the existence of metastable states on the number of flavors. The variation of the effective potential on the number of flavors was discussed in Refs. [3,10]. It has been shown in these references that as the number of flavors increases, the free energy density of metastable vacua increases at any temperature. For $N_f \geq 3$, no metastability at any temperature was seen. However, these are essentially perturbative calculations that are not applicable near T_c. In the PQM model discussed here, the flavor dependence comes from the third term in the effective potential V_{eff} [Eq. (13)]. The parameters of the linear sigma model potential part in Eq. (13) are fixed to reproduce the results of chiral symmetry restoration for $N_f = 2$. For simplicity, we take this linear sigma model part in Eq. (13) for different values of N_f. For the Polyakov loop part of the potential in Eq. (13), the parameter T_0 depends on the number of flavors and chemical potential as in [17],

$$T_0(\mu, N_f) = T_\tau e^{-1/(\alpha_0 b(\mu))}. \tag{28}$$

Here,

$$b(\mu) = \frac{1}{6\pi}(11N_c - 2N_f) - b_\mu \frac{\mu^2}{T_\tau^2} \tag{29}$$

where $T_\tau = 1.770$ GeV, $\alpha_0 = 0.304$, and $b_\mu = 16N_f/\pi$. The flavor dependence of the effective potential normalized by T^4 is shown in Fig. 8 for $\mu = 0$ and $T = 400$ MeV. As may be noted from Fig. 8, the absolute value of the free energy difference between the true vacuum ($\theta = 0$) and the minima at nonzero θ increases with the flavor number. It may also be noted that beyond $N_f \geq 3$, the metastable minima become unphysical as the pressure becomes negative. Such an observation was also noted in Refs. [3,10] within a perturbative approach. For higher temperatures also we did not find any metastable state (up to $T = 600$ MeV).

B. Metastable states at finite chemical potential

From Eq. (25), it is clear that there is a nonvanishing contribution from the imaginary part of $\Omega_{\bar{q}q}$ at finite chemical potential [23]. However, as argued in Ref. [23], we neglect this part in our calculation at finite temperature so that the effective potential is real where a minimization procedure can be applied. The critical temperature decreases as chemical potential increases as seen in [17]. The variation of both the order parameters at different chemical potentials with respect to temperature is the same as seen in [17]. The free energy density of true vacuum at finite chemical potential is more negative than the same at zero chemical potential at any temperature greater than the critical temperature. But, the energy density of $Z(3)$ metastable vacua at finite chemical potential increases compared to zero chemical potential. Hence, the threshold temperature for metastability increases with the chemical potential. The temperature T_m beyond which the $Z(3)$ metastable vacuum arises is shown as a function of chemical potential in Fig. 9.

Here, we have taken the temperature parameter T_0 for the Polyakov loop potential to have a μ dependence as given in Eq. (28). From Fig. 9, one can see that the metastability temperature remains almost constant ($T_m = 310$ MeV) up to $\mu = 170$ MeV and it increases beyond $\mu = 170$ MeV. Generally, the metastability temperature should increase with the increase in chemical potential since we are adding more dynamical quark degrees of freedom by increasing the chemical potential; however, the cause for this sharp increase of metastability temperature beyond $\mu = 170$ MeV is not very clear. We expect that there must be drastic change in phase transition dynamics beyond this chemical potential. It has been already observed that the critical point exists at $(T_c, \mu_c) = (150\text{ MeV}, 168\text{ MeV})$ [17]. When the

chemical potential is less than the critical chemical potential, it is a crossover in the QCD phase diagram. Beyond critical chemical potential, there is a first-order phase transition between the confined and deconfined phases where the dynamics of the phase transition are very different than the crossover. So, the temperature dependence of metastable states at higher chemical potential might reveal the phase transition dynamics and hints at the existence of a critical point. These metastable states have a phase of 115° as already seen for zero chemical potential.

IV. PHASE TRANSITION KINETICS AND NUMERICAL SIMULATION

The thermalization time scale at RHIC is very small (~0.2 fm). In this short time scale an equilibrium dynamics of the transition from confined phase to deconfined phase appears very unlikely. Hence in this work, we carry out a $2+1$ dimensional field theoretical simulation of the dynamics of the confinement-deconfinement transition in a quench as in Ref. [11]. Here we use the framework of Bjorken's boost invariant longitudinal expansion model [27] for the central rapidity region in relativistic heavy ion collisions. To model the quench, we take the initial field configuration to constitute a small patch around $\Phi = 0$, which corresponds to confining vacuum configuration near zero temperature. We take the initial phase of Φ to vary randomly between 0 and 2π from one lattice site to the other, while the magnitude of Φ is taken appropriately to obtain the $Z(3)$ domain structure. In principle, the initial magnitude of Φ (i.e., $\epsilon = 0.1 \times \mathrm{VEV}$) should be smaller than the vacuum expectation value (VEV) of Φ at $\mathrm{T_{max}} = 400$ MeV (i.e., maximum temperature obtained at LHC).

This initial field configuration, which represents the equilibrium field configuration of a system with $\mathrm{T} \ll \mathrm{T}_c$, is evolved using the effective potential with $\mathrm{T} = \mathrm{T_{max}} > \mathrm{T}_c$. This represents the transition dynamics of a quench. Here, we will compare the two different cases:

(i) Polyakov potential with an explicit symmetry-breaking term as in Eq. (27).
(ii) PQM model effective potential as given in Eq. (13).

First we will consider the situation of the Polyakov loop potential with an explicit symmetry-breaking term as given in Eq. (27). The kinetic energy term for the Polyakov loop field is represented by $\frac{\mathrm{N}}{g^2}|\partial_\mu \Phi|^2 \mathrm{T}^2$. The field configuration of the Polyakov loop field is evolved by the time-dependent equation of motion in the Minkowski space as appropriate for Bjorken's longitudinal scaling model [28]:

$$\frac{\partial^2 \Phi_j}{\partial \tau^2} + \frac{1}{\tau}\frac{\partial \Phi_j}{\partial \tau} - \frac{\partial^2 \Phi_j}{\partial x^2} - \frac{\partial^2 \Phi_j}{\partial y^2} = -\frac{g^2}{2\mathrm{NT}^2}\frac{\partial V_{\mathrm{eff}}}{\partial \Phi_j}; \quad j = 1, 2, \tag{30}$$

with $\Phi = \Phi_1 + i\Phi_2$. The evolution of the field was numerically implemented by a stabilized leapfrog algorithm of second-order accuracy both in space and in time with the second-order derivatives of Φ approximated by a diamond-shaped grid. Here, we have used a square lattice of 2000×2000 points and the physical size of the lattice is 20 fm. Hence, the lattice spacing is $\Delta x = 0.01$ fm. We take $\Delta t = \Delta x/\sqrt{2}$ to satisfy the Courant stability criteria. The stability and accuracy of the simulation is checked using the conservation of energy during simulation. The total energy fluctuations remain a few percent without any net increase or decrease of total energy in the absence of the dissipative term $\dot{\Phi}$ in the equation of motion. This is the only dissipative term used here due to Bjorken's longitudinal expansion. Here the temperature varies as $\tau^{-1/3}$ due to Bjorken's longitudinal expansion.

It has already been shown that for a very small explicit symmetry-breaking term with $b_1 = 0.005$ (for a first-order phase transition), $Z(3)$ domains are formed via bubble nucleation, then expand, and $Z(3)$ walls and strings are produced [14]. $Z(3)$ domains also have been studied in a quench scenario with this symmetry-breaking term, where it has been seen that the true vacuum domain dominates over the other two $Z(3)$ metastable domains [11]. However, in this work as mentioned in the previous section, we consider the case with $b_1 = 0.1$, which is suitable for a crossover transition between the confined and deconfined phase at zero chemical potential. With this symmetry-breaking term, the plot of the potential along true and metastable vacua is given in Fig. 7. As we have mentioned earlier, the potential along metastable vacua is higher compared to true vacuum near the origin $\Phi = 0$. So, if we choose the initial patch for the Polyakov loop field near $\Phi = 0$ to be very small, i.e., $\epsilon = 0.01 \times \mathrm{VEV}$, then the field always rolls down to the true vacuum. In this case, we do not get any $Z(3)$ domain structures in the simulation.

The patch size for the initial configuration of the Polyakov loop depends upon the flatness of the potential near $\Phi = 0$ (Polyakov correlation length) at a temperature less than the critical temperature. The initial Polyakov loop field can take large value for a flat potential near $\Phi = 0$ compared to a narrow potential. We choose a larger initial patch, i.e., $\epsilon = 0.1 \times \mathrm{VEV}$ for this potential; the field already sits on the top of the barrier along the metastable vacua near $\Phi = 0$. Then the field rolls down to all vacua. Since the potential is more tilted towards the true vacuum, the larger fraction of the region is occupied by domains of true vacuum inside, as shown in Fig. 10. Here, we have shown the values of the phase of Φ around the three $Z(3)$ vacua in terms of different colors (shades) to focus on the evolution of the $Z(3)$ domain structure. Thus all the values of the phase θ of Φ are separated into three ranges, between $-2\pi/6$ and $2\pi/6$ ($\theta = 0$ vacuum), between $2\pi/6$ and π ($\theta = 2\pi/3$ vacuum), and between π and $-2\pi/6$ ($\theta = 4\pi/3$ vacuum). As the field evolves, the angular variation of Φ becomes less random over small length scales, leading to a sort of $Z(3)$ domain structure. $Z(3)$ domains become more

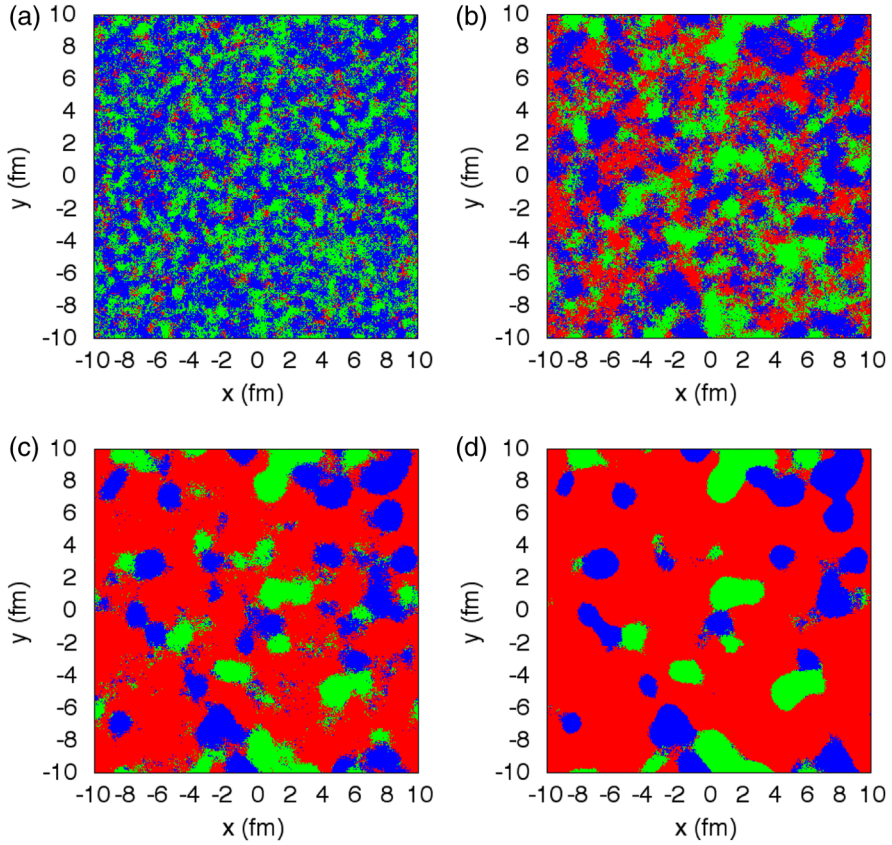

FIG. 10. Field configurations at different times with explicit symmetry-breaking effect. The shading (color) representing the dominant region in (d) corresponds to the true vacuum with $\theta = 0$. (a)–(d) show the growth of domains for $\tau = 1.2$, 1.6, 2.2, and 2.4 fm (with corresponding values of temperature T = 368, 335, 311, and 298 MeV), respectively.

well defined and grow in size by coarsening, as shown in the sequence of figures in Fig. 10. The boundaries of different $Z(3)$ domains represent $Z(3)$ walls, and the junction of three different $Z(3)$ domains gives rise to the QGP strings.

Here, we would like to mention that at temperature 400 MeV as shown in Fig. 7, the potential along the metastable vacuum has a small barrier between the confined vacuum and metastable vacuum. So, there is a possibility of metastable domain formation via bubble nucleation. Since the barrier height is much smaller than the energy density difference between the confined and metastable vacua, these will be thick wall bubbles. But, there is no barrier between confined vacuum and true vacuum at this temperature and true vacuum domains are formed due to the roll down of the Polyakov loop field. Hence, this raises a new possibility of $Z(3)$ domain formation where the transition dynamics are different along different vacua. We would like to study this in detail in the future.

Next, we discuss the situation for the PQM model. The plots of the potential for this model along true and metastable vacua at T = 400 MeV have been shown in Fig. 7. It is clear from the figure that the energy density difference between the true and metastable vacua of this model is very large compared to the previous case with $b_1 = 0.1$. Since it is a large explicit symmetry-breaking case for V_{eff}, with the initial field configuration mentioned above for $b_1 = 0.1$ (i.e., $\epsilon = 0.1 \times \text{VEV}$), the field Φ always rolls down completely along the $\theta = 0$ vacuum. There is no metastable domain formation for this case. When the field always rolls down to true vacuum, it has been observed that large field oscillations lead to large fluctuations in the evolution of flow anisotropies in the quench case compared to the equilibrium transition case [11]. We expect similar results for this case as in [11]. Here, the order parameter σ is a dynamic field which evolves as the Polyakov loop field in the quench scenario. The initial field configuration for σ is chosen appropriately (VEV value ~93.0 MeV at zero temperature and sigma value fluctuating around this value from one lattice site to another). The equations of motion for the two order parameters are now coupled through V_{eff}. While the dynamical equation for the Polyakov loop order parameter is given by Eq. (30), the equation of motion for the σ field is given by

$$\frac{\partial^2\sigma}{\partial\tau^2} + \frac{1}{\tau}\frac{\partial\sigma}{\partial\tau} - \frac{\partial^2\sigma}{\partial x^2} - \frac{\partial^2\sigma}{\partial y^2} = -\frac{\partial V_{\text{eff}}}{\partial\sigma}. \tag{31}$$

Here we would like to study true vacuum and sigma domain growth in a noncentral collision. It is a limitation of the current study to use hydrodynamic simulation. In contrast to the previous case, here we use a more realistic temperature profile of Woods-Saxon shape with the size in the X and Y directions being different and representing an elliptical shape for a noncentral collision. The Woods-Saxon temperature profile is given by the following:

$$\mathrm{T}(r) = \mathrm{T}_{\mathrm{center}}/[1 + \exp[(r - R)/a]], \qquad (32)$$

where $\mathrm{T}_{\mathrm{center}}$ is the temperature at the center of the QGP region. R represents the radius of the elliptical QGP region for the noncentral collision and $a = 0.56$ fm is the thickness of the transition layer to the vacuum. Here r represents the distance from the center of the lattice at which temperature is measured using the above equation. At $\tau = 1$ fm (the thermalization time scale used here), the temperature at the center of the QGP region is $\mathrm{T}_{\mathrm{center}} = 400$ MeV. This allows us to have a well-defined size for the central QGP region, with temperature smoothly decreasing at the boundary of this region [11]. The transverse size R of this system is taken to increase with uniform acceleration of 0.015 c per fm, starting from an initial value of R [29]. The initial transverse expansion velocity is taken to be zero. This expanding background of the temperature profile is supposed to represent the hydrodynamically expanding quark gluon plasma. The central temperature of the Woods-Saxon profile is taken to decrease by assuming that the total entropy (integrated in the transverse plane) decreases linearly as appropriate for the Bjorken dynamics of longitudinal expansion. The physical lattice size is 30 fm × 30 fm. The Woods-Saxon temperature profile (representing the QGP region) is taken to have a diameter of about 16 fm as appropriate for Au-Au collision for RHICEs. The large physical size of the lattice allows for the evolution of the QGP region to be free from boundary effects. Here we have taken the eccentricity of the QGP region to be 0.8. We have presented the Polyakov loop and sigma domain growth at time $\tau = 3$ fm in Fig. 11. Figure 11(a) represents the true vacuum domain and Fig. 11(b) presents sigma domain growth at $\tau = 3$ fm, respectively. Here the ringlike structure at the boundary of the noncentral QGP region represents the large fluctuations in the field value due to the huge temperature gradient corresponding to the tail part of the Woods-Saxon temperature profile. However, we are only interested in the domain growth inside the QGP region (neglecting the boundary effects). The background is in the confined phase (outside of the elliptical QGP region). So, the Polyakov loop field and sigma field value outside the QGP region are accordingly in the confined phase.

We also study the variation of the average Polyakov loop and sigma field (normalized with respect to vacuum) over the whole lattice with τ as shown in Fig. 12. This is very important to study the relaxation behavior of the Polyakov loop and sigma field in a quenched scenario. The average Polyakov loop and sigma field over the lattice are defined as

$$\langle|\Phi|\rangle = \frac{1}{N^2}\sum_{l,m}|\Phi|_{l,m} \quad \text{and} \quad \langle\sigma\rangle = \frac{1}{N^2}\sum_{l,m}\sigma_{l,m}. \qquad (33)$$

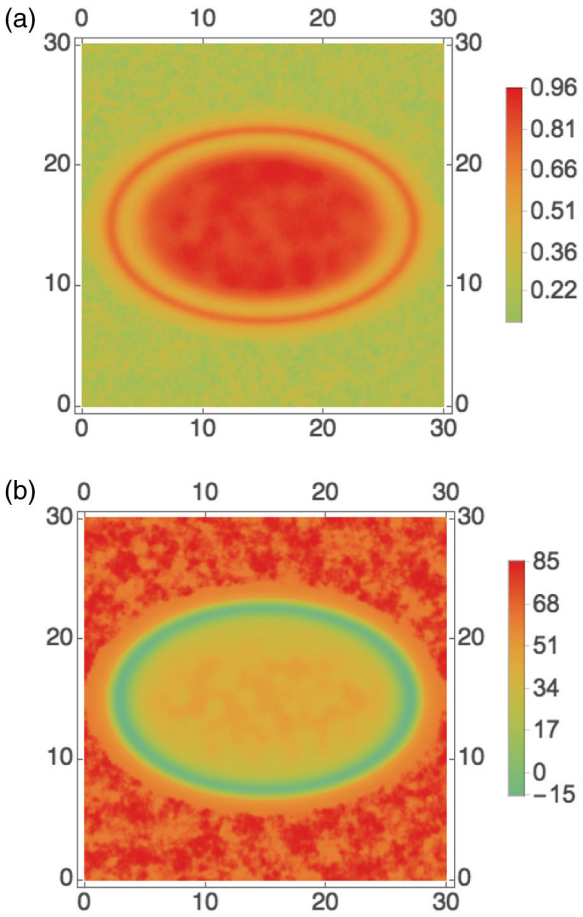

FIG. 11. (a) Polyakov loop. (b) Sigma field (in units of MeV) domain growth at $\tau = 3$ fm.

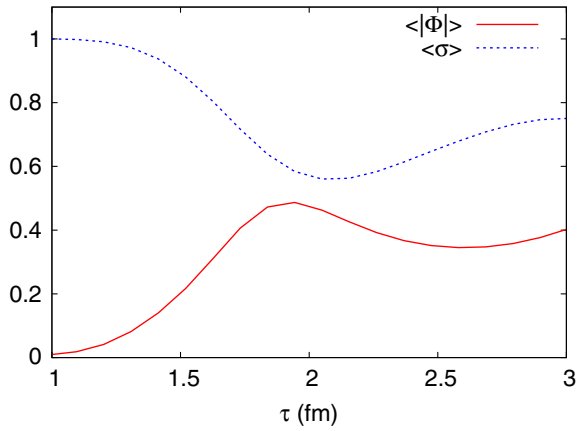

FIG. 12. Plot of average Polyakov loop and normalized sigma field value with τ.

Here N represents the number of lattice points in one direction and (l,m) represents the coordinates of the lattice. We can observe from Fig. 12 that the average Polyakov loop initially increases up to $\tau = 2$ fm, approaching the equilibrium value; however, at the same time, temperature decreases with τ due to longitudinal expansion and the equilibrium value of the Polyakov decreases as temperature decreases. Hence, there is a turnover after $\tau = 2$ fm where the Polyakov loop decreases. This is also the case for the normalized sigma field value, where it initially decreases, approaching the equilibrium value, and increases slightly after $\tau = 2$ fm. We would like to point out that the central temperature is $T_{center} = 313$ MeV at $\tau = 2$ fm and there is a large fraction of the lattice which is at low temperature due to the Woods-Saxon temperature profile. We would also like to point out that as the temperature decreases further at $\tau = 3$ fm, the shape of the effective potential is very flat near the minimum. So, the equilibrium value of the Polyakov loop oscillates slightly near the VEV, which is shown as an increase in the Polyakov loop around $\tau = 3$ fm.

As we have described above for $b_1 = 0.1$, there is a possibility of $Z(3)$ metastable domain formation via bubble nucleation due to the barrier between false vacuum and $Z(3)$ metastable vacuum for this case in the PQM model. However, here the barrier height is of the same order as the energy density difference between confined vacuum and metastable vacua at a temperature 400 MeV, as shown in Fig. 7. But, there is no barrier between false vacuum and true vacuum at this temperature. So, there is a possibility of $Z(3)$ domain formation in this model via mixed transition dynamics, i.e., roll-down of the Polyakov loop field along true vacuum and bubble nucleation along metastable vacua. One needs to calculate the nucleation probability for this bubble formation and to study the phase transition dynamics with a suitable bubble profile as in [13,14]. We would like to study this case in the future.

V. CONCLUSIONS

We have presented the possibility of the existence of $Z(3)$ metastable states in the PQM model. The metastable states exist for the Polyakov loop potential with large barriers between different $Z(3)$ vacua. The metastable vacua are not present near the critical temperature, but they appear around temperature 310 MeV at zero chemical potential due to the strong explicit symmetry-breaking effect of quarks. There is also a shift in the phase of metastable vacua and they appear at 115° and 245°, respectively. This explicit symmetry-breaking effect in the PQM model is strong compared to the small explicit breaking effect of quarks discussed in different Polyakov loop models [6]. We have observed that this metastability temperature remains almost constant up to finite chemical 170 MeV, and it increases after this chemical potential. This might be due to the difference in phase transition dynamics after the critical chemical potential 170 MeV. The phase transition between the confined and deconfined phase is a crossover up to the critical chemical potential and it is a first-order phase transition beyond this chemical potential. In other words, one can say that the metastability temperature as a function of chemical potential is sensitive to the phase transition dynamics.

It has been suggested that $Z(3)$ domains give a microscopic explanation for the large color opacity (jet quenching) and near perfect fluidity (small value of η/s) of QGP [9,10]. Therefore, it is very important to study these domains near the critical temperature in effective models like the PQM or Polyakov loop extended Nambu-Jona-Lasinio (PNJL) model. We expect the results will be similar in the PNJL model. Here we have observed in a quench scenario that due to strong explicit symmetry breaking of quarks in the PQM model, there is no metastable domain formation. The whole region is occupied only by a true vacuum domain. Hence, it is very unlikely to explain jet quenching or the perfect fluidity of QGP due to $Z(3)$ domains in the PQM model. However, this nature of the QGP can be described well in models with a small explicit symmetry-breaking effect of quarks.

ACKNOWLEDGMENTS

We are very grateful to Ajit M. Srivastava for very useful discussions and suggestions. We also thank Arpan Das and Ananta P. Mishra for useful discussions. We would like to thank Ananta P. Mishra for providing the code of energy minimization to get the interface profile.

[1] M. Wilde (ALICE Collaboration), Nucl. Phys. **A904–905**, 573c (2013); C. Shen, U. Heinz, J.-F. Paquet, and C. Gale, Phys. Rev. C **89**, 044910 (2014).
[2] L. D. McLerran and B. Svetitsky, Phys. Rev. D **24**, 450 (1981); B. Svetitsky, Phys. Rep. **132**, 1 (1986).
[3] V. Dixit and M. C. Ogilvie, Phys. Lett. B **269**, 353 (1991).
[4] V. M. Belyaev, I. I. Kogan, G. W. Semenoff, and N. Weiss, Phys. Lett. B **277**, 331 (1992).
[5] P. N. Meisinger and M. C. Ogilvie, Phys. Lett. B **379**, 163 (1996).

[6] A. Dumitru and R. D. Pisarski, Phys. Lett. B **504**, 282 (2001); Phys. Rev. D **66**, 096003 (2002); Nucl. Phys. **A698**, 444 (2002).
[7] A. Dumitru, D. Roder, and J. Ruppert, Phys. Rev. D **70**, 074001 (2004); T. Banks and A. Ukawa, Nucl. Phys. **B225**, 145 (1983); F. Green and F. Karsch, Nucl. Phys. **B238**, 297 (1984); P. N. Meisinger and M. C. Ogilvie, Phys. Rev. D **52**, 3024 (1995).
[8] M. Deka, S. Digal, and A. P. Mishra, Phys. Rev. D **85**, 114505 (2012).
[9] M. Asakawa, S. A. Bass, and B. Muller, Phys. Rev. Lett. **110**, 202301 (2013).
[10] K. Kashiwa and A. Monnai, Phys. Rev. D **89**, 011501(R) (2014).
[11] R. K. Mohapatra and A. M. Srivastava, Phys. Rev. C **88**, 044901 (2013).
[12] B. Layek, A. P. Mishra, and A. M. Srivastava, Phys. Rev. D **71**, 074015 (2005); B. Layek, A. P. Mishra, A. M. Srivastava, and V. K. Tiwari, Phys. Rev. D **73**, 103514 (2006).
[13] U. S. Gupta, R. K. Mohapatra, A. M. Srivastava, and V. K. Tiwari, Phys. Rev. D **82**, 074020 (2010).
[14] U. S. Gupta, R. K. Mohapatra, A. M. Srivastava, and V. K. Tiwari, Phys. Rev. D **86**, 125016 (2012).
[15] A. P. Mishra, A. M. Srivastava, and V. K. Tiwari, Indian J. Phys. B **85**, 1161 (2011).
[16] A. Atreya, A. Sarkar, and A. M. Srivastava, Phys. Rev. D **85**, 014009 (2012).
[17] B.-J. Schaefer, J. M. Pawlowski, and J. Wambach, Phys. Rev. D **76**, 074023 (2007).
[18] C. Herold, M. Nahrgang, I. Mishustin, and M. Bleicher Phys. Rev. C **87**, 014907 (2013).
[19] A. Singh, S. Puri, and H. Mishra, Nucl. Phys. **A864**, 176 (2012); **A908**, 12 (2013); Europhys. Lett. **102**, 52001 (2013).
[20] C. Ratti, M. A. Thaler, and W. Weise, Phys. Rev. D **73**, 014019 (2006).
[21] K. Kajantie, L. Karkkainen, and K. Rummukainen, Nucl. Phys. **B357**, 693 (1991).
[22] S. Roessner, C. Ratti, and W. Weise, Phys. Rev. D **75**, 034007 (2007).
[23] B. W. Mintz, R. Stiele, R. O. Ramos, and J. S. Bielich, Phys. Rev. D **87**, 036004 (2013).
[24] V. Koch, arXiv:9706075.
[25] B. J. Schaefer and M. Wagner, Phys. Rev. D **85**, 034027 (2012).
[26] S. Roessner, T. Hell, C. Ratti, and W. Weise, Nucl. Phys. **A814**, 118 (2008).
[27] J. D. Bjorken, Phys. Rev. D **27**, 140 (1983).
[28] T. C. Petersen and J. Randrup, Phys. Rev. C **61**, 024906 (2000).
[29] P. F. Kolb, J. Sollfrank, and U. Heinz, Phys. Rev. C **62**, 054909 (2000).